

Published in final edited form as:

Curr Biol. 2009 February 24; 19(4): 287–296. doi:10.1016/j.cub.2009.01.055.

Spindle Fusion Requires Dynein-Mediated Sliding of Oppositely Oriented Microtubules

Jesse C. Gatlin^{1,2}, Alexandre Matov⁴, Aaron C. Groen^{1,3}, Daniel J. Needleman^{1,3}, Thomas J. Maresca^{1,2}, Gaudenz Danuser⁴, Timothy J. Mitchison^{1,3}, and E.D. Salmon^{1,2}

¹Cell Division Group, Marine Biological Laboratory, Woods Hole, MA 02543, USA

²Department of Biology, University of North Carolina at Chapel Hill, Chapel Hill, NC 27599, USA

³Department of Systems Biology, Harvard Medical School, Boston, MA 02115, USA

⁴Department of Cell Biology, Laboratory for Computational Cell Biology, The Scripps Research Institute, La Jolla, CA 92037, USA

Summary

Background—Bipolar spindle assembly is critical for achieving accurate segregation of chromosomes. In the absence of centrosomes, meiotic spindles achieve bipolarity by a combination of chromosome initiated microtubule nucleation/stabilization and motor driven organization of microtubules. Once assembled, the spindle structure is maintained on a relatively long time scale despite the high turnover of the microtubules that comprise it. To study the underlying mechanisms responsible for spindle assembly and steady-state maintenance, we used microneedle manipulation of pre-assembled meiosis II spindles in *Xenopus* egg extracts.

Results—By bringing two bipolar spindles close together, firm linkages formed between overlapping peripheral spindle microtubules that pulled the spindles into bipolar alignment. The adjacent poles fused together more slowly once the poles and metaphase plates were aligned ultimately resulting in a single spindle of nearly normal size and shape. Alignment and fusion were both blocked when cytoplasmic dynein function was inhibited, indicating a critical role for this motor in both these processes. Two proximal monopolar microtubule arrays, generated by inhibiting kinesin 5 (Eg5), pulled themselves into a single monopole using a dynein-dependent mechanism providing the plus ends of microtubules extending from opposite poles overlapped each other.

Conclusions—Our experiments illustrate the architectural plasticity of the spindle and reveal a robust ability of the system to attain a bipolar morphology. We hypothesize that a major mechanism driving spindle fusion is dynein-mediated sliding of oppositely-oriented microtubules, a novel function for the motor, and posit that this same mechanism might also be involved in normal spindle assembly and homeostasis.

Introduction

Establishing and maintaining a bipolar steady-state in microtubule assembly dynamics is critical for chromosome segregation, since two spindle poles define a single axis of force

© 2009 Elsevier Inc. All rights reserved

Correspondence: Jesse (Jay) C. Gatlin Phone: 919 962-2354 Fax: 919 962-1625 E-mail: E-mail: jgatlin@email.unc.edu.

Publisher's Disclaimer: This is a PDF file of an unedited manuscript that has been accepted for publication. As a service to our customers we are providing this early version of the manuscript. The manuscript will undergo copyediting, typesetting, and review of the resulting proof before it is published in its final citable form. Please note that during the production process errors may be discovered which could affect the content, and all legal disclaimers that apply to the journal pertain.

generation during anaphase. During spindle assembly microtubules are nucleated from centrosomal and non-centrosomal sources, requiring cells to integrate microtubules nucleated at multiple, spatially distinct sites into a single bipolar array [1,2]. Interestingly, if groups of chromosomes are initially far enough apart at entry into mitosis/meiosis or are physically separated from one another, they each can form bipolar spindles which are capable of fusing into a single metaphase spindle [3,4]. In this case, achieving bipolarity in the final metaphase spindle requires adjacent spindles to align all chromosomes onto a single equatorial plate and to reduce the total number of poles to two. Similar microtubule-dependent mechanisms may also be important for chromosome alignment within an individual bipolar spindle as kinetochores can initiate microtubule formation and elongation independent of the spindle pole [5-7].

The fusion of two preassembled spindles is likely controlled by the same fundamental mechanisms that govern normal spindle assembly and steady state maintenance. In acentrosomal female animal meiosis, spindle assembly results from motor-dependent organization of microtubules nucleated and stabilized around chromatin [1]. Two microtubule motors in particular, kinesin 5 (Eg5) and cytoplasmic dynein/dynactin (dynein) make important mechanistic contributions. Eg5 is a homotetrameric motor that crosslinks and slides oppositely oriented microtubules apart where they overlap at the spindle mid-zone [8,9]. This activity drives microtubule minus ends poleward and contributes substantially to microtubule poleward flux [10-12]. In contrast to Eg5, the minus end-directed motor complex dynein contains multiple microtubule-binding domains that likely bind to the same microtubule [13]. Thus, the dynein complex must form multimeric complexes or associate with other proteins in order to crosslink and slide microtubules.

In *Xenopus* egg extract spindles, dynein antagonizes Eg5 in regulating spindle morphology and length. Strong inhibition of Eg5 by the small molecule inhibitor monastrol causes collapse of metaphase spindles into radial, monopolar microtubule arrays [14,15] whereas perturbation of dynein function results in splaying of spindle poles and, depending on the means of inhibition, spindle elongation [15-17]. Consistent with opposing functions, inhibiting both motors results in bipolar spindles of nearly normal length and shape, but structurally very fragile [15]. Recently proposed “slide and cluster” models posit that new microtubules are continuously formed near chromosomes in meiotic spindles (presumably by a RanGTP-regulated pathway [18]) and moved with their minus ends leading toward one or the other pole by Eg5 sliding [19]. As a result, microtubule minus ends are distributed throughout the spindle [20]. It is thought that these ends may be the attachment sites dynein uses to oppose Eg5-mediated poleward microtubule sliding, but exactly how and where dynein acts to antagonize Eg5 are not known.

We reasoned that by studying the interaction of two preassembled spindles we may gain new insight into the mechanistic basis of microtubule motor function within the spindle. We found that bipolar spindles will indeed fuse if brought close enough together with microneedles and do so in distinct ways depending on their initial spatial arrangement. Fusion also occurred between closely opposed pairs of Eg5-inhibited monopoles. In both cases, fusion depended on dynein function. Based on these observations and additional analyses of microtubule dynamics during fusion, we propose a model in which dynein generates pulling forces between poles by sliding microtubules of opposite polarity. Our results suggest a novel function for the dynein motor that has implications for meiotic spindle morphogenesis and length regulation.

Results

Nearby spindle pairs align and fuse with each other

We first tested how two spindles interact if their axes were parallel to each other and their ends overlapped as shown in Figure 1 (see also Supplemental Data, Videos 1 & 2). Once two spindles were manipulated to touch each other and held there for ~30s or more, they adhered strongly, and became impossible to pull apart by micromanipulation without distortion of both spindles. In this parallel orientation the spindles indeed fused and did so by sliding, where the proximal, overlapped poles moved apart, increasing the length of the overlap until the spindles eventually aligned pole-to-pole (Figure 1A, B). During parallel spindle sliding, antiparallel microtubule overlap between adjacent spindles is expected to be maximal when the spindles are half-overlapped with a pole of each spindle aligned with the equator of the other. As the spindles slide further together, the amount of antiparallel overlap should decrease. Assuming the motors responsible for spindle fusion rely on a specific orientation of interacting microtubules (e.g. Eg5 or dynein), then one might expect sliding velocity to vary as a function of overlap. The average velocity of sliding was determined from the slopes of linear regressions of the plots shown in Figure 1C and found to be $1.2 \pm 0.4 \mu\text{m}/\text{min}$ ($n = 9$ spindle pairs, minimum $R^2 = 0.91$). This value did not vary significantly as the amount of overlap changed (Figure 1D).

Spindle poles, decorated with fluorescently labeled antibodies against NuMA, remained largely intact during spindle alignment by sliding, while chromosomes, visualized using DAPI, demonstrated persistent alignment on the equator of each spindle during sliding. Lateral movements of poles and chromosomes completed fusion of the two spindles into one, a process that usually occurred more slowly than sliding alignment of the metaphase plates (Figure 1A). Following spindle fusion, the resultant microtubule array was always a bipolar spindle. On average, these spindles were ~10% longer than the initial two spindles (Figure S1A; [21]). Interestingly, the microtubule content of the resulting steady-state structures, as measured by integrated fluorescence intensity of spindle-incorporated labeled tubulin, was approximately half the total content of the sum of its two predecessors (Figure S1B).

We then tested if antiparallel spindle microtubule interactions were required for efficient fusion of two adjacent spindles. This was done by placing one spindle axis orthogonal to the other (“T-bone” geometry, Figure 2A,B; see also Supplemental Data, Video 3). In this geometry, initial movement of the proximal poles towards each other was coupled to a rotation of one or both spindles, which brought their axes closer to parallel (with one exception; $n=17$ spindle pairs). The two spindles then slid into alignment, similar to spindles positioned in parallel with pole overlap as in Figure 1. We refer to the rotational component of spindle alignment as “jackknifing”.

Pulling forces on peripheral spindle microtubules contribute to spindle fusion

Spindle jackknifing suggests the existence of traction forces between poles. We reasoned that these forces were the result of motor-mediated sliding of interacting microtubules extending from each pole. Although not evident using low power objectives, higher resolution, confocal imaging of fluorescently labeled tubulin (Figure 3A) or EB1 (Figure 3B; Supplemental Data, Video 4) revealed a low density of peripheral microtubules that radiate outwards from the spindle poles at all angles to the spindle axis. To test if these microtubules could pull poles together and to estimate their distance of action, we positioned spindles end-to-end with their interpolar axes aligned and their proximal poles separated by various distances (Figure 3D, schematic in 3E). The critical distance for interaction in this geometry was ~10 microns; spindles this far apart or closer typically interacted and moved to bring their proximal poles together, while spindles further apart typically did not (Figure 3E). In 8/10 cases, the proximal poles fused and then one or both spindles pivoted around the now shared pole, and jackknifed

to form a single bipolar spindle (Fig 3D). In 2/10 cases, the proximal poles moved together but then continued to slide past each other, aligning by the sliding mode shown in Figure 1. Spindles positioned side-by-side with various separation distances and orientations of their interpolar axes also fused when sufficiently close (the two closest poles within $\sim 35\mu\text{m}$; Figure S2). We suspect the critical interaction distance depends on spindle orientation because peripheral microtubules are longer extending from the pole outward away from the sides of the spindle compared to those extending away from the back of the pole (Figure 3A,B,C).

Bipolar spindle alignment and fusion require cytoplasmic dynein

Pole focusing mechanisms are typically mediated by minus-end directed motors. In *Xenopus* egg extracts there are two prominent motors with this directional polarity: cytoplasmic dynein and XCTK2, a member of kinesin-14 family of motors [22]. To investigate the possible role of either motor in spindle fusion, we first treated fully assembled bipolar spindles with $25\mu\text{M}$ Na_3VO_4 (vanadate) prior to micromanipulation and asked what effect this would have on bipolar fusion. This vanadate concentration has been shown to inhibit cytoplasmic dynein motor activity with no measureable effect on that of XCTK2 [23]. As expected for dynein inhibition, vanadate caused spindle widening of the poles and an increase in spindle length that occurred at a rate of $\sim 5\mu\text{m}/\text{min}$, the rate overlapping microtubules slid apart within the spindle (by fluorescent speckle microscopy, data not shown) [16,19]. This concentration of vanadate completely inhibited alignment and fusion of parallel, overlapped spindles ($n = 11$ spindle pairs; Figure 4A; Supplemental Data, Video 5). Unlike controls, in many instances two spindles pushed and held together for $\sim 30\text{s}$ simply drifted apart when the microneedles were removed suggesting the formation of adhesive linkages between the two spindles was either slowed or did not occur altogether.

To rule out non-specific effects of vanadate, we used two alternative approaches to inhibit dynein function. In the first, monoclonal antibody against the 70.1 kDa dynein intermediate chain (ab70.1) was added to extract containing fully assembled spindles. As previously shown [24], ab70.1 caused bipolar spindles to lose focus at the poles, elongate, and ultimately transform into barrel-shaped microtubule arrays with aligned chromosomes at their midpoint (Figure 4B; Supplemental Data, Video 6). Similar to vanadate-treated spindles, when these microtubule arrays were juxtaposed with no discernible space between the structures, they failed to adhere, align and fuse (Figure 4B, $n = 8$ spindle pairs). Spindle assembly following dynein immunodepletion from the extract ($>97\%$, as determined by western blot, Figure S3) resulted in similar barrel-shaped spindles and had the same inhibitory effect on fusion ($n = 9$ spindle pairs; Figure 4C; Supplemental Data, Video 7). In contrast, in extracts depleted of the minus end-directed motor XCTK2, a condition which still allows for relatively normal bipolar spindle assembly [22], spindle-spindle adhesion and sliding were unaffected ($n = 6$ spindle pairs from 2 different extracts; Figure 4D; Supplemental Data, Figure S3, Video 8) although, qualitatively, pole fusion seemed to occur more slowly.

Dynein slides overlapping microtubules of opposite polarity

To further examine the role of dynein in spindle fusion, we assembled monopolar asters by inhibiting Eg5 using small molecule inhibitors that block ADP release and mimic loss of function of the motor (monastrol and the more potent drug S-trityl-L-cysteine [STLC]) [10, 25]. When two such monopoles were brought sufficiently close together by manipulation, they interacted, moved together at rates of $2.8 \pm 0.8\mu\text{m}/\text{min}$, and fused into a single monopole (for velocity measurements, $n = 8$ monopole pairs; the total number monopole fusion observations was > 20 ; Figure 5A; Supplemental Data, Video 9). As they merged together, we often observed an increase in birefringence between the two poles which had a spindle-like shape, but the formation of this central spindle was variable in its occurrence as shown in Figure 5A. The maximum initial interpolar separation that permitted merging was $\sim 60\mu\text{m}$ (Figure 5C, control).

Analysis of monopole size, as measured by tracking growing plus ends with fluorescent EB1, revealed a marked decrease in the number of plus ends extending beyond a radius of 35 μm (Figure 5D), suggesting that overlap of plus ends is necessary to facilitate fusion. Interestingly, only one plus end (out of 1396 tracked) was found beyond 55 μm from the monopole center. Therefore, it is unlikely that long microtubules spanning from one monopole center to other are required for fusion, although we cannot rule out the possibility that during fusion, antiparallel overlap stabilizes microtubule dynamics thereby generating some tubules that extend beyond this distance. Similar to bipoles, monopole fusion was completely inhibited by 25 μM vanadate ($n = 9$ monopole pairs; Figure 5B, C; Supplemental Data, Video 10). Importantly, this treatment did not appreciably change monopole size (i.e. diameter, data not shown) and overlap of microtubules near the edges of monopoles was evident provided the initial separation distance was less than $\sim 60 \mu\text{m}$. Alternative methods to inhibit dynein, like those employed in our bipole fusion experiments, proved problematic with Eg5-inhibited monopoles (see Supplemental Information). In summary, the results of the monopole fusion experiments are consistent with the hypothesis that pulling forces are generated by a mechanism involving dynein motor activity and associated crosslinking to slide and pull together oppositely oriented polar microtubules.

Based on this hypothesis, we made two predictions, the first about dynein localization and the second about microtubule movements resulting from dynein-dependent crosslinking. In regards to localization, our monopole fusion experiments predicted that the motor should be present near the periphery of monopolar arrays, not simply at their poles. Indeed this is the case, although the labeling is weak relative to kinetochores and the pole, dynein does co-localize with tubulin throughout the structure (Figure 5E). To address microtubule movement resulting from antiparallel microtubule interactions we added a low level (125 nM) of fluorescently labeled EB-1 to assembled monopoles (as in Figure 5D) and viewed monopole fusion using high resolution confocal microscopy (Figure 5F) [26]. As EB-1 tracks only the plus ends of growing microtubules, our analysis was limited to this subpopulation of microtubules. We reasoned that pulling forces generated at intersection points lying off the interpolar axis would result in movement of the interacting microtubules toward the axis. In individual monopoles, the tracks of EB1 comets generally radiate outward from a single point (Figure 5D, Supplemental Data, Video 11), but during the initial stages of monopole fusion we observed EB1 comet trajectories with transverse movements toward the interpolar axis (Figure 5F,G; Supplemental Data, Video 12). Importantly, this “clustering” of microtubules indicates that forces generated at distal sites along the microtubules are transmitted to the rest of the microtubule array. Furthermore, this bundling occurred in a region away from chromosomes and associated kinetochores, thus excluding involvement of kinetochore-associated dynein [27] or parallel sliding of kinetochore-nucleated microtubules [28].

Discussion

The defined orientation of microtubules within monopolar arrays [12,24,29] and the sensitivity of fusion to dynein perturbation (Figure 5B), allow us to postulate that the microtubule-microtubule interactions responsible for fusion occur between oppositely oriented microtubules and are mediated by dynein. This represents an additional functional geometry for dynein motor complexes which contrasts the prevailing view in the literature: that dynein-mediated focusing of microtubule minus ends into poles occurs largely via sliding and transport of microtubules of the same polarity [24,30-32]. In this sliding model, dynein pulls the minus end of one microtubule towards the minus end of another, as originally proposed by Karsenti and colleagues to explain taxol aster formation in *Xenopus* egg extracts [33]. This parallel sliding is thought to be mediated by dynein-NuMA complexes localized at or near microtubule minus ends [24,34]. Our immunofluorescence data shows that dynein localizes throughout monopolar microtubule arrays, even towards the more distal aspects of the array near

presumptive microtubule plus ends (Figure 5E). It is possible that minus ends are distributed throughout the monopole as well [19,20], and because this distribution is not known, our experiments do not resolve clearly where (or how) dynein complexes are bound along the microtubules they slide. However, dynein has been shown to localize to growing plus ends [35-37] presumably to better position the motor to capture its intended targets. It is possible that these dynein-dependent forces are somehow coupled to plus end polymerization dynamics, perhaps explaining why taxol-induced asters in *Xenopus* egg extracts do not fuse and instead form tessellated patterns in the plane of the coverslip surface (T.J. Mitchison unpublished observations). Alternatively, dynein complexes capable of crosslinking microtubules might bind all along the walls of existing microtubules using unknown accessory proteins other than NuMA. Future analyses are needed to characterize the nature of this binding, which is critically important in understanding how this sliding filament mechanism might contribute to spindle assembly and length maintenance [38,39].

Based on our data, we propose a model whereby the primary mechanism driving spindle fusion is dynein-dependent pulling forces between overlapping polar microtubule arrays that extend radially from focused poles. These forces alone can readily explain both monopole fusion and the jackknifing mode of bipole fusion (Figure 6). For monopoles, dynein crosslinks oppositely oriented microtubules from both arrays generating a tensile force that pulls the poles together. Because Eg5 is inhibited, the poles slide together and ultimately merge. During jackknifing, where the axis of one spindle is initially perpendicular to the other, the same forces pull the closest two poles together first, likely because the shorter distance stochastically favors higher peripheral microtubule density and a larger number of force-generating interactions between overlapped peripheral microtubule arrays. At the same time, the spindle rotates in the direction dictated by the highest torque which is generated by dynein-dependent pulling forces between the overlapped peripheral microtubule arrays from the distal poles.

If pole-pole attraction is the dominant mechanism responsible for fusion, it seems somewhat paradoxical that the proximal poles slide away from each other when spindles are positioned with their axes parallel and poles overlapped (i.e. during spindle sliding; Figure 1). This can be explained, however, providing the overlapped geometry allows for pulling forces to be generated between the proximal pole of each spindle and the distal pole of the other (see “F_{OUTER}” in Figure 6B) and that these forces, in sum, are greater than the pulling force between the two proximal poles (“F_{INNER}” in Figure 6B). Alternatively, spindle sliding may occur because kinesin-5/Eg5 is concentrated on spindle microtubules near the poles [40,41] with its plus end-directed motility acting to antagonize dynein minus end-directed motility, significantly reducing the net pulling force between the proximal poles. Although this latter explanation is plausible, we favor the former mechanism because bipolar spindle sliding did not occur when dynein alone was inhibited (see Figure 4).

The same forces responsible for pair-wise bipole and monopole fusion might also be at work within a single bipolar spindle, affecting steady state spindle length by antagonizing Eg5 sliding. Indeed, the observation that Eg5 and dynein antagonize one another to regulate *Xenopus* extract spindle length is consistent with this idea [15,19]. Furthermore, our observation that bipolar spindle sliding occurs at a velocity that is slower than that observed in vitro for unloaded dynein ($\sim 75 \mu\text{min}^{-1}$, [42]) or dynein-dependent sliding of parallel microtubules in the spindle ($\sim 6 \mu\text{min}^{-1}$, [18]) might be a result of this antagonism, however, it could also be due to effects of molecular friction and viscous drag (although the drag forces at the sliding speeds observed are likely to be negligible). Interestingly, monopole fusion occurred at a faster rate than bipole sliding, $2.8 \pm 0.8 \mu\text{min}^{-1}$ and $1.2 \pm 0.4 \mu\text{min}^{-1}$ respectively ($p \ll 0.05$). It is also possible that interactions between peripheral microtubules and those within the spindle are regulated differently due to spatial and/or geometric parameters. This could explain why dynein forces seem to dominate antiparallel interactions

between peripheral microtubules during bipolar spindle fusion (where both motors are active), whereas those forces generated by Eg5 dominate within the spindle, particularly near the midzone, as evident by persistent microtubule flux. Indeed, spatial variations of Eg5 dynamics within the spindle have been characterized [40,41]. Consistent with this idea, the motor's activity has been shown to be positively affected by RanGTP and its downstream effectors [43] which form a gradient around chromosomes at the metaphase plate [44]. Alternatively, the oblique angles made by intersecting peripheral microtubules might favor force generation by a given motor type over another.

Independent of the molecular mechanisms, spindle fusion demonstrates the remarkable architectural plasticity of the spindle and provides unique insight into how this property might be governed. That the post-fusion spindle is approximately the same size as its predecessors demonstrates steady state spindle size is only modestly affected by a doubling of the chromosomal number, an observation consistent with others in the literature [21,45]. The fact that spindles maintain some sense of their own structural identity during pair-wise fusion, with aligned chromosomes and focused poles, suggests a constancy of form unaffected by predicted changes in the shape of putative signaling gradients localized around chromosomes, at least over the time scale of fusion. This adds credence to the idea that once assembled and organized, the microtubules of the spindle themselves provide structural “feedback” that helps to maintain spindle shape, possibly due to microtubule-dependent nucleation of microtubules within the spindle [46].

Experimental Procedures

Reagents

All reagents, unless stated otherwise, were purchased from Sigma-Aldrich (St. Louis, MO) and are of the highest quality available.

Spindle assembly in *X. laevis* egg extracts

CSF-arrested egg extracts were prepared as described by Murray and colleagues [47,48]. “Cycled” spindles, prepared as described in [48], were allowed to assemble for 1-1.5 hrs at 18°C before experimentation. Monopolar spindles were assembled in the presence of STLC (25uM) or monastrol (100uM), both small molecule inhibitors of Eg5. A comparison of monopoles in each condition revealed no discernable differences in architecture or behavior during fusion experiments.

Spindle Micromanipulation and Imaging

To prepare micromanipulation chambers, 22mm² coverslips were used to cover circular cut-outs (~3/4” diameter) in custom-made metal slides (3”×1”×1/32”). The #1.5 coverslip (Fisher Scientific) was adhered to a pre-heated slide using melted VALAP (1:1:1 vasoline, lanolin, paraffin) applied around the cut-out. The assembly was allowed to cool and a small aliquot (~5-7μl) of extract was spread over the glass surface with a pipette tip and overlaid with paraffin oil (~300μl) to prevent the sample from drying out during subsequent imaging.

Micromanipulation experiments were conducted on a TE2000e inverted microscope stand (Nikon) equipped with a motorized microscope stage (Applied Scientific Instrumentation). Dual pneumatic micromanipulators (Narishige) were mounted directly to the condenser arm of the microscope and adjusted so the opposing needles entered the well at shallow angles to the coverslip surface. The borosilicate glass needles used for micromanipulation were made using a model P-97 micropipette puller (Sutter Instrument Company). The needles had long, tapered ends (~9mm from base of taper to the needle tip) and were lowered through the paraffin oil overlay and into the extract for manipulation. Polarization optics (i.e. a crossed polarizer

and analyzer) in combination with a 20x differential interference contrast (DIC) objective (Nikon Plan Fluor, 20x/0.75 NA MImm) were used to visualize spindles during micromanipulation. The needles were readily visible under these imaging conditions. Images were acquired using a cooled CCD camera (Orca-ER; Hamamatsu) or a cooled EM-CCD camera (iXon; Andor).

For real-time imaging during spindle fusion, the multimode data acquisition feature of Metamorph software (Molecular Devices) was used to control image acquisition. The positions of poles were tracked with either the “track object” or “track points” applications in Metamorph. Where needed, rotation of acquired image stacks was performed using custom Matlab software (Mathworks) written by J.C. Gatlin. Unless otherwise state, at least three different extracts were used for each experimental condition.

Various fluorescently labeled antibodies and proteins were used to see specific spindle elements during real-time imaging of spindle fusion. To visualize spindle poles for fusion velocity measurements, Alexa Fluor-488 (Invitrogen) labeled anti-NuMA antibody [49] was added to extracts (final concentration of 10 μgml^{-1}) before spindle assembly. Growing plus ends were marked by recombinant EB1 (125 nM) directly labeled with the same dye and added to extracts prior to imaging [26]. Peripheral microtubules were labeled by incorporation of Alexa Fluor 647-tubulin ($\sim 100 \text{ ngml}^{-1}$) added to assembled spindles. DAPI ($1 \mu\text{gml}^{-1}$) was also added to some extracts to view chromosomes during fusion. High resolution digital images were collected using a cooled CCD Orca ER camera coupled to a Yokogawa spinning disk confocal unit (CSU10, PerkinElmer) and mounted on a TE300 inverted microscope (Nikon). A 60x Plan Apochromat, 1.4 NA DIC objective was used for all high resolution imaging. The system was controlled using Metamorph software.

Samples were prepared for indirect-immunofluorescence as described previously [48] with only minor changes. Briefly, assembled monopoles were fixed using paraformaldehyde, pelleted onto coverslips, and then postfixed in - 20°C methanol. Following rehydration in PHEM + 0.1% TritonX-100 (TX), the coverslips were blocked in PHEM + 5% boiled donkey serum for 30min to 1hr. Samples were then incubated in blocking buffer with primary antibodies against α -tubulin (rat polyclonal, Serotec) and 70-74kD intermediate chain of cytoplasmic dynein ([50], a generous gift from K. Vaughan). After three rinses in blocking buffer, samples were incubated for 1hr in blocking buffer with fluorophoreconjugated secondary antibodies (Invitrogen), rinsed three times in PHEM-TX, mounted on slides in mounting buffer (20mM Tris pH 8.0, 0.5% N-propyl gallate, 90% Glycerol), and sealed with nail polish.

Immunodepletions and dynein perturbation

To immunodeplete proteins from egg extracts, antibodies were first bound to protein-A-conjugated magnetic beads (Invitrogen). A 300 μl volume of bead suspension was rinsed three times in *Xenopus* buffer (XB; 10mM K-Hepes (pH 7.7), 100 mM KCl, 1 mM MgCl_2 , 0.1 mM CaCl_2 , and 50 mM sucrose). For each immunodepletion, 90 μg of antibody was added to the equivalent of 300 μl of the original bead suspension and allowed to conjugate overnight with end-over-end rotation at 4°C. Antibody-conjugated beads were rinsed 3x and resuspended in 300 μl XB. Beads from 100 μl of this suspension were resuspended in 150 μl of CSF-arrested extract and incubated for 1hr on ice with occasional gentle agitation. The beads were collected on ice for 10min to facilitate complete retrieval from the viscous extract. The remaining partially depleted extract was then used to resuspend a new 100 μl aliquot of antibody-conjugated beads and the process repeated for a total of three immunodepletions. Cycled spindle assembly reactions were carried out in the immunodepleted extracts as described above. The antibodies used for these experiments were a monoclonal antibody anti-74kD dynein intermediate chain (IgG isotype; Chemicon) and a rabbit polyclonal anti-XCTK2 [22].

For dynein perturbation studies, vanadate (25 μ M) was added to extracts from 100mM stock. For antibody perturbation, concentrated anti-70.1kD DIC antibody (Sigma Aldrich) was added to extracts containing preassembled spindles to 1 mgml⁻¹ with a volume ratio of 1:10 [18]. Imaging of spindle fusion was typically started 5-10min after the addition of either reagent.

Determination of monopole size by EB1 tracking

Individual EB1 spot features were identified and localized in all images using a scale-space theory based three step band-pass detection algorithm [51]. Feature tracking was accomplished by single particle tracking as described in [52] where Kalman filtering was used to project particle paths for more robust particle association between frames. The center of the monopole was determined as the center of mass of the pair-wise intersections between the axes extrapolated from all Alexa Fluor 488-EB1 tracks present in a frame. To compensate for drift in the monopole spindle position over time, we updated the pole center coordinates in every time-point of the movie and performed further analysis relative to this position. All programs for Alexa Fluor 488-EB1 feature analysis and graphical representation were written in the Danuser laboratory in MATLAB (Mathworks, Natick, MA) and C++.

Statistical Analyses

All statistical analyses and graphing were done using Microsoft Excel software. Reported results are mean values \pm standard deviations.

Supplementary Material

Refer to Web version on PubMed Central for supplementary material.

Acknowledgments

We thank L. Cameron (Dana-Farber Cancer Institute, A. Joglekar (University of North Carolina at Chapel Hill) and S. Dumont (Harvard Medical School) for helpful discussions, comments, and critical reading of the manuscript as well as other members of the Salmon Laboratory and the Cell Division Group. We also thank K. Vaughan (University of Notre Dame) for the generous gift of anti-dynein intermediate chain antibody. A special thanks goes to H. Luther (MBL) and M. Peterson (MBL) for help with acquiring necessary equipment. This work was supported by National Institute of General Medicine grants to J.C. Gatlin (F32GM080049), E.D. Salmon (GM24364 and GM60678), and to G. Danuser (GM60678). T.J. Mitchison was funded by the National Cancer Institute (CA078048-09).

References

1. Walczak CE, Heald R. Mechanisms of mitotic spindle assembly and function. *Int Rev Cytol* 2008;265:111–158. [PubMed: 18275887]
2. O'Connell CB, Khodjakov AL. Cooperative mechanisms of mitotic spindle formation. *J Cell Sci* 2007;120:1717–1722. [PubMed: 17502482]
3. Savoian MS, Rieder CL. Mitosis in primary cultures of *Drosophila melanogaster* larval neuroblasts. *J Cell Sci* 2002;115:3061–3072. [PubMed: 12118062]
4. Church K, Nicklas RB, Lin HP. Micromanipulated bivalents can trigger mini-spindle formation in *Drosophila melanogaster* spermatocyte cytoplasm. *J Cell Biol* 1986;103:2765–2773. [PubMed: 3098743]
5. Maiato H, Rieder CL, Khodjakov A. Kinetochore-driven formation of kinetochore fibers contributes to spindle assembly during animal mitosis. *J Cell Biol* 2004;167:831–840. [PubMed: 15569709]
6. Tulu US, Fagerstrom C, Ferenz NP, Wadsworth P. Molecular requirements for kinetochore-associated microtubule formation in mammalian cells. *Curr Biol* 2006;16:536–541. [PubMed: 16527751]
7. Torosantucci L, De Luca M, Guarguaglini G, Lavia P, Degraffi F. Localized RanGTP Accumulation Promotes Microtubule Nucleation at Kinetochores in Somatic Mammalian Cells. *Mol Biol Cell* 2008;19:1873–1882. [PubMed: 18287525]

8. Sharp DJ, Yu KR, Sisson JC, Sullivan W, Scholey JM. Antagonistic microtubule-sliding motors position mitotic centrosomes in *Drosophila* early embryos. *Nat Cell Biol* 1999;1:51–54. [PubMed: 10559864]
9. Kapitein LC, Peterman EJ, Kwok BH, Kim JH, Kapoor TM, Schmidt CF. The bipolar mitotic kinesin Eg5 moves on both microtubules that it crosslinks. *Nature* 2005;435:114–118. [PubMed: 15875026]
10. Miyamoto DT, Perlman ZE, Burbank KS, Groen AC, Mitchison TJ. The kinesin Eg5 drives poleward microtubule flux in *Xenopus laevis* egg extract spindles. *J Cell Biol* 2004;167:813–818. [PubMed: 15583027]
11. Shirasu-Hiza M, Perlman ZE, Wittmann T, Karsenti E, Mitchison TJ. Eg5 causes elongation of meiotic spindles when flux-associated microtubule depolymerization is blocked. *Curr Biol* 2004;14:1941–1945. [PubMed: 15530396]
12. Mitchison TJ, Maddox P, Groen A, Cameron L, Perlman Z, Ohi R, Desai A, Salmon ED, Kapoor TM. Bipolarization and poleward flux correlate during *Xenopus* extract spindle assembly. *Mol Biol Cell* 2004;15:5603–5615. [PubMed: 15385629]
13. Ross JL, Wallace K, Shuman H, Goldman YE, Holzbaur EL. Processive bidirectional motion of dynein-dynactin complexes in vitro. *Nat Cell Biol* 2006;8:562–570. [PubMed: 16715075]
14. Mayer TU, Kapoor TM, Haggarty SJ, King RW, Schreiber SL, Mitchison TJ. Small molecule inhibitor of mitotic spindle bipolarity identified in a phenotype-based screen. *Science* 1999;286:971–974. [PubMed: 10542155]
15. Mitchison TJ, Maddox P, Gaetz J, Groen A, Shirasu M, Desai A, Salmon ED, Kapoor TM. Roles of polymerization dynamics, opposed motors, and a tensile element in governing the length of *Xenopus* extract meiotic spindles. *Mol Biol Cell* 2005;16:3064–3076. [PubMed: 15788560]
16. Yang G, Houghtaling BR, Gaetz J, Liu JZ, Danuser G, Kapoor TM. Architectural dynamics of the meiotic spindle revealed by single-fluorophore imaging. *Nat Cell Biol* 2007;9:1233–1242. [PubMed: 17934454]
17. Gaetz J, Kapoor TM. Dynein/dynactin regulate metaphase spindle length by targeting depolymerizing activities to spindle poles. *J Cell Biol* 2004;166:465–471. [PubMed: 15314063]
18. Heald R, Tournibize R, Blank T, Sandaltzopoulos R, Becker P, Hyman A, Karsenti E. Self-organization of microtubules into bipolar spindles around artificial chromosomes in *Xenopus* egg extracts. *Nature* 1996;382:420–425. [PubMed: 8684481]
19. Burbank KS, Mitchison TJ, Fisher DS. Slide-and-cluster models for spindle assembly. *Curr Biol* 2007;17:1373–1383. [PubMed: 17702580]
20. Burbank KS, Groen AC, Perlman ZE, Fisher DS, Mitchison TJ. A new method reveals microtubule minus ends throughout the meiotic spindle. *J Cell Biol* 2006;175:369–375. [PubMed: 17088423]
21. Brown KS, Blower MD, Maresca TJ, Grammer TC, Harland RM, Heald R. *Xenopus tropicalis* egg extracts provide insight into scaling of the mitotic spindle. *J Cell Biol* 2007;176:765–770. [PubMed: 17339377]
22. Walczak CE, Verma S, Mitchison TJ. XCTK2: a kinesin-related protein that promotes mitotic spindle assembly in *Xenopus laevis* egg extracts. *J Cell Biol* 1997;136:859–870. [PubMed: 9049251]
23. Shimizu T, Toyoshima YY, Edamatsu M, Vale RD. Comparison of the motile and enzymatic properties of two microtubule minus-end-directed motors, ncd and cytoplasmic dynein. *Biochemistry* 1995;34:1575–1582. [PubMed: 7849016]
24. Heald R, Tournibize R, Habermann A, Karsenti E, Hyman A. Spindle assembly in *Xenopus* egg extracts: respective roles of centrosomes and microtubule self-organization. *J Cell Biol* 1997;138:615–628. [PubMed: 9245790]
25. Groen AC, Needleman D, Brangwynne C, Gradinaru C, Fowler B, Mazitschek R, Mitchison TJ. A novel small-molecule inhibitor reveals a possible role of kinesin-5 in anastral spindle-pole assembly. *J Cell Sci* 2008;121:2293–2300. [PubMed: 18559893]
26. Timauer JS, Grego S, Salmon ED, Mitchison TJ. EB1-microtubule interactions in *Xenopus* egg extracts: role of EB1 in microtubule stabilization and mechanisms of targeting to microtubules. *Mol Biol Cell* 2002;13:3614–3626. [PubMed: 12388761]
27. Pfarr CM, Coue M, Grissom PM, Hays TS, Porter ME, McIntosh JR. Cytoplasmic dynein is localized to kinetochores during mitosis. *Nature* 1990;345:263–265. [PubMed: 2139717]

28. Khodjakov A, Copenagle L, Gordon MB, Compton DA, Kapoor TM. Minus-end capture of preformed kinetochore fibers contributes to spindle morphogenesis. *J Cell Biol* 2003;160:671–683. [PubMed: 12604591]
29. Kapoor TM, Mayer TU, Coughlin ML, Mitchison TJ. Probing spindle assembly mechanisms with monastrol, a small molecule inhibitor of the mitotic kinesin, Eg5. *J Cell Biol* 2000;150:975–988. [PubMed: 10973989]
30. Tulu US, Rusan NM, Wadsworth P. Peripheral, non-centrosome-associated microtubules contribute to spindle formation in centrosome-containing cells. *Curr Biol* 2003;13:1894–1899. [PubMed: 14588246]
31. Gaetz J, Gueroui Z, Libchaber A, Kapoor TM. Examining how the spatial organization of chromatin signals influences metaphase spindle assembly. *Nat Cell Biol* 2006;8:924–932. [PubMed: 16892054]
32. Chakravarty A, Howard L, Compton DA. A mechanistic model for the organization of microtubule asters by motor and non-motor proteins in a mammalian mitotic extract. *Mol Biol Cell* 2004;15:2116–2132. [PubMed: 14978218]
33. Verde F, Berrez JM, Antony C, Karsenti E. Taxol-induced microtubule asters in mitotic extracts of *Xenopus* eggs: requirement for phosphorylated factors and cytoplasmic dynein. *J Cell Biol* 1991;112:1177–1187. [PubMed: 1671864]
34. Merdes A, Heald R, Samejima K, Earnshaw WC, Cleveland DW. Formation of spindle poles by dynein/dynactin-dependent transport of NuMA. *J Cell Biol* 2000;149:851–862. [PubMed: 10811826]
35. Vaughan KT, Tynan SH, Faulkner NE, Echeverri CJ, Vallee RB. Colocalization of cytoplasmic dynein with dynactin and CLIP-170 at microtubule distal ends. *J Cell Sci* 1999;112(Pt 10):1437–1447. [PubMed: 10212138]
36. Lee WL, Oberle JR, Cooper JA. The role of the lissencephaly protein Pac1 during nuclear migration in budding yeast. *J Cell Biol* 2003;160:355–364. [PubMed: 12566428]
37. Han G, Liu B, Zhang J, Zuo W, Morris NR, Xiang X. The *Aspergillus* cytoplasmic dynein heavy chain and NUDF localize to microtubule ends and affect microtubule dynamics. *Curr Biol* 2001;11:719–724. [PubMed: 11369237]
38. McIntosh JR, Hepler PK, Van Wie DG. Model for Mitosis. *Nature* 1969;224:659–663.
39. Nedelec F. Computer simulations reveal motor properties generating stable antiparallel microtubule interactions. *J Cell Biol* 2002;158:1005–1015. [PubMed: 12235120]
40. Kapoor TM, Mitchison TJ. Eg5 is static in bipolar spindles relative to tubulin: evidence for a static spindle matrix. *J Cell Biol* 2001;154:1125–1133. [PubMed: 11564753]
41. Uteng M, Hentrich C, Miura K, Bieling P, Surrey T. Poleward transport of Eg5 by dynein-dynactin in *Xenopus laevis* egg extract spindles. *J Cell Biol* 2008;182:715–726. [PubMed: 18710923]
42. Paschal BM, Vallee RB. Retrograde transport by the microtubule-associated protein MAP 1C. *Nature* 1987;330:181–183. [PubMed: 3670402]
43. Wilde A, Lizarraga SB, Zhang L, Wiese C, Gliksman NR, Walczak CE, Zheng Y. Ran stimulates spindle assembly by altering microtubule dynamics and the balance of motor activities. *Nat Cell Biol* 2001;3:221–227. [PubMed: 11231570]
44. Kalab P, Pralle A, Isacoff EY, Heald R, Weis K. Analysis of a RanGTP-regulated gradient in mitotic somatic cells. *Nature* 2006;440:697–701. [PubMed: 16572176]
45. Wuhr M, Chen Y, Dumont S, Groen AC, Needleman DJ, Salic A, Mitchison TJ. Evidence for an upper limit to mitotic spindle length. *Curr Biol* 2008;18:1256–1261. [PubMed: 18718761]
46. Mahoney NM, Goshima G, Douglass AD, Vale RD. Making microtubules and mitotic spindles in cells without functional centrosomes. *Curr Biol* 2006;16:564–569. [PubMed: 16546079]
47. Murray AW. Cell cycle extracts. *Methods Cell Biol* 1991;36:581–605. [PubMed: 1839804]
48. Desai, A.; Murray, AW.; Mitchison, T.; Walczak, CE. *Methods in Cell Biology*. Vol. Volume 61. Academic Press; 1999. The Use of *Xenopus* Egg Extracts to Study Mitotic Spindle Assembly and Function; p. 385–412.
49. Groen AC, Cameron LA, Coughlin M, Miyamoto DT, Mitchison TJ, Ohi R. XRHAMM functions in ran-dependent microtubule nucleation and pole formation during anastral spindle assembly. *Curr Biol* 2004;14:1801–1811. [PubMed: 15498487]

50. Vaughan PS, Leszyk JD, Vaughan KT. Cytoplasmic dynein intermediate chain phosphorylation regulates binding to dynactin. *J Biol Chem* 2001;276:26171–26179. [PubMed: 11340075]
51. Matov, A.; Danuser, G.; Wittmann, T. Measuring Full Microtubule Dynamic Instability Using Growth Marker. In submission
52. Yang, G.; Matov, A.; Danuser, G. Reliable Tracking of Large Scale Dense Antiparallel Particle Motion for Fluorescence Live Cell Imaging; IEEE Int'l Conference on Computer Vision and Pattern Recognition, Workshop on Computer Vision Methods for Bioinformatics; 2005.

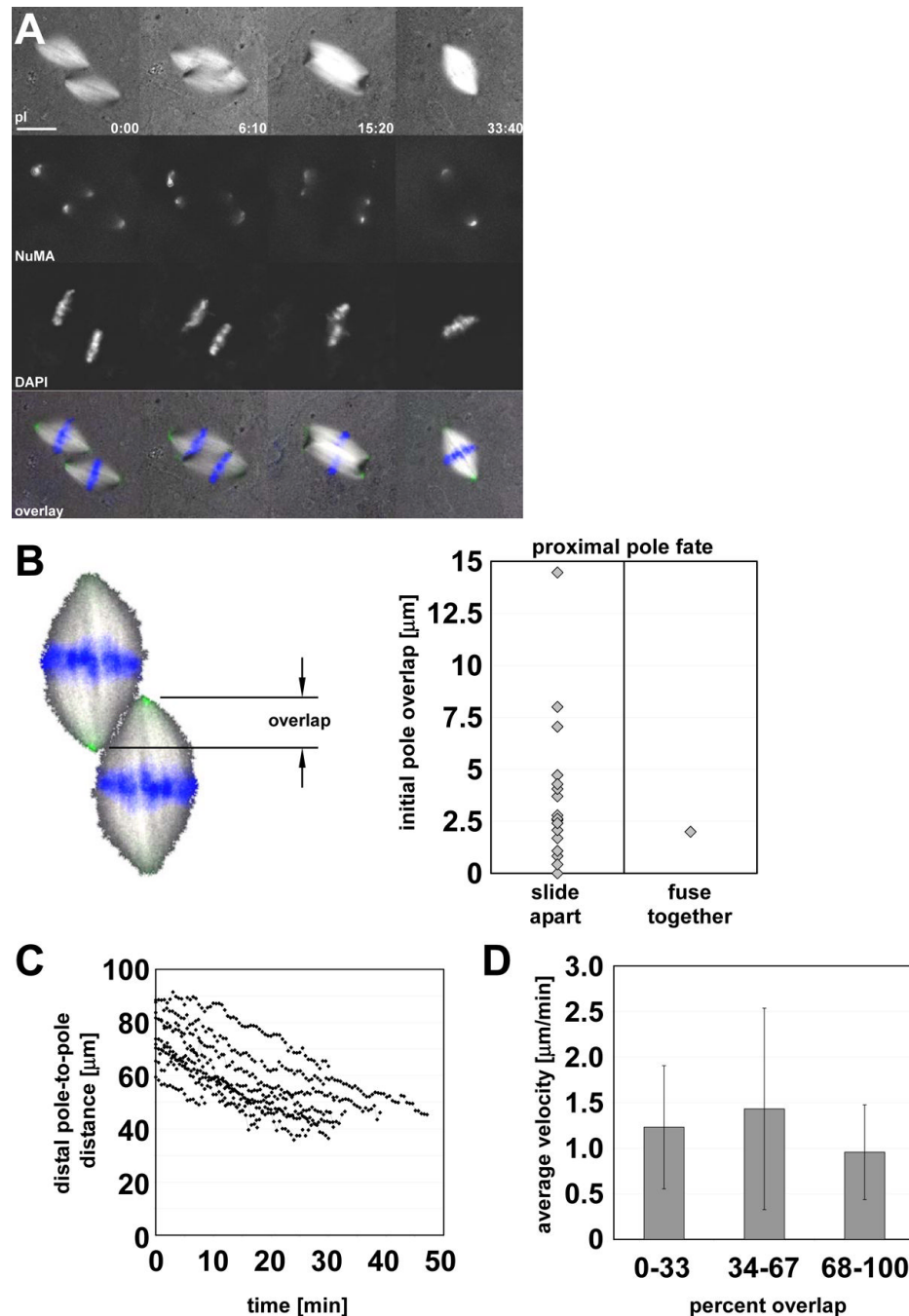


Figure 1. Parallel spindles with overlapped poles merge by sliding

Meiosis II arrested bipolar spindles were positioned using microneedles with their interpolar axes parallel and with overlapped proximal poles. Subsequent alignment and fusion was monitored using polarization optics and fluorescence microscopy (**A**). Directly labeled anti-NuMA antibodies were added to the extracts to mark the poles and DAPI was used to label the chromosomes at the metaphase plate. In this starting configuration, the majority of spindles fused by sliding parallel to the interpolar axis (**A,B**). In **C**, the position of the distal poles is plotted versus time. For all time courses, the zero time point represents the time the first image was acquired following spindle positioning. This typically occurred within a few seconds after moving the microneedles away from the spindles. The average velocity of alignment (the slope)

is $1.2 \pm 0.4 \mu\text{m}/\text{min}$ ($n = 9$ spindle pairs). For **D**, the same data as in **C** was used to determine the velocity as a function of percent overlap (i.e. $100 \times \text{overlap}/\text{average initial spindle length}$). Values were obtained by averaging the slopes of linear regressions for sliding that occurred during the fraction of overlap indicated. Analysis using a pairwise Student's t-test indicated no statistically significant differences between the velocities (all $p > 0.05$). All scale bars represent $25 \mu\text{m}$.

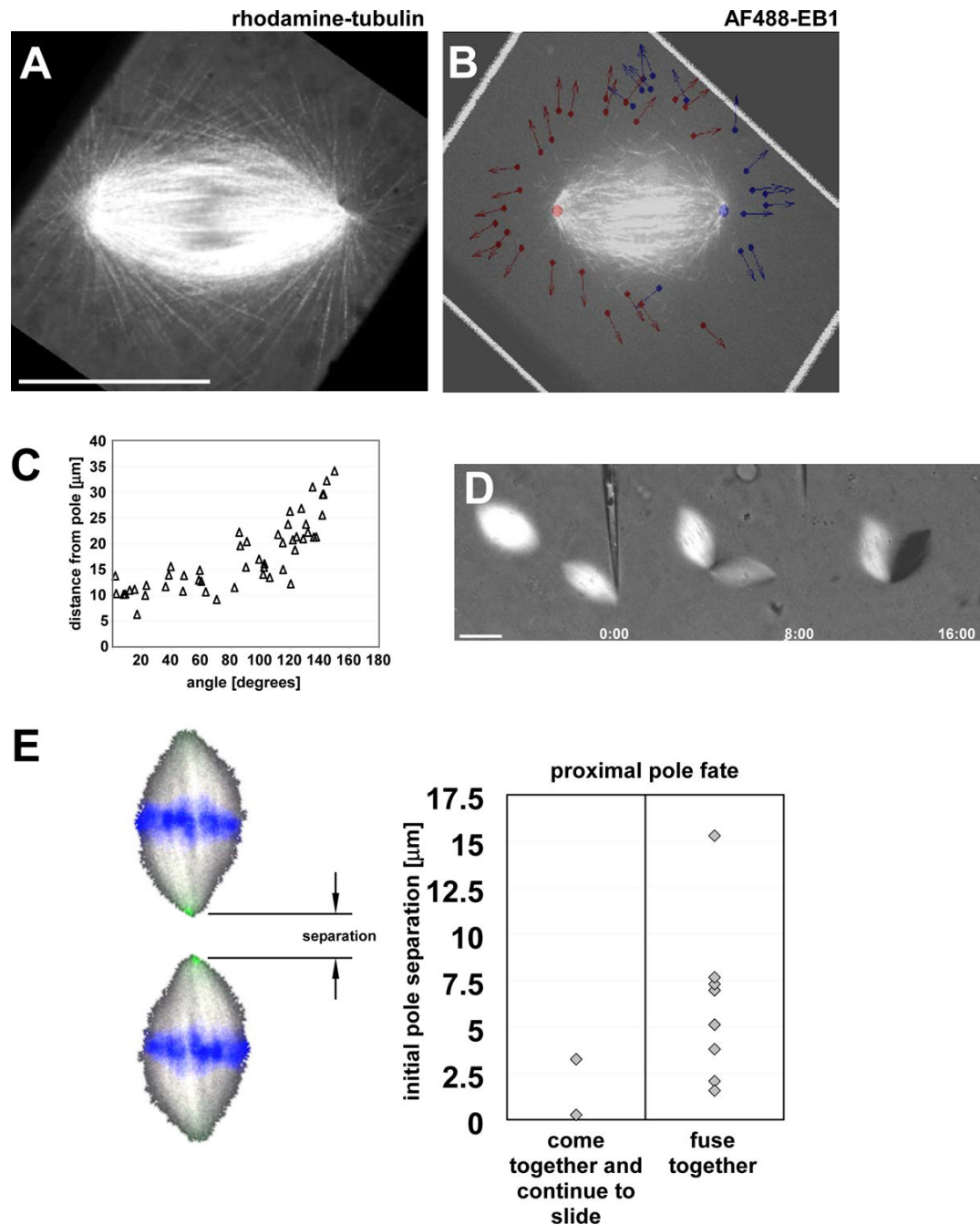


Figure 3. Peripheral microtubules facilitate spindle alignment and fusion through a distance
 High resolution confocal imaging of rhodamine-tubulin labeled spindles reveals numerous peripheral microtubules extending beyond the circumference of the main spindle body, **A**. In **B**, complementary studies using fluorescently labeled EB-1 (125 nM) added to pre-assembled spindles to visualize the dynamics of growing microtubule ends also show peripheral microtubule extending beyond the margins of the spindle. The image shown in **B** represents a single frame from a time-lapse series spanning ~ 2 minutes (result is typical of the $n = 20$ spindles observed). The centers of overlaid circles mark the most distal positions of EB1 trajectories observed during imaging whereas the arrows indicate the direction of EB1 comet trajectories. Colors indicate from which pole the growing microtubule likely emanated from.

This was determined by assuming a linear trajectory for each EB1 comet and finding the point where it intersected a line running through both spindle poles (i.e. the extended interpolar axis). The pole closest to this point was assumed to be the originating pole. In some cases, the comet trajectories did not intersect with the extended interpolar axis, so we assumed the comet originated from the nearest pole. The distances from the poles to each EB1 comet were plotted against the angle of the comet trajectory to the horizontal, with 0° oriented on the horizontal extending behind the pole and 180° on the horizontal toward the metaphase plate (**C**). To test whether spindles could merge through a distance, spindle pairs were positioned on the same axis with separation between their proximal poles (**D**). In most cases, the spindles first came together, fused at their proximal poles, and then pivoted or “jackknifed” around the shared pole (**D**, **E**). Scale bars = 25µm.

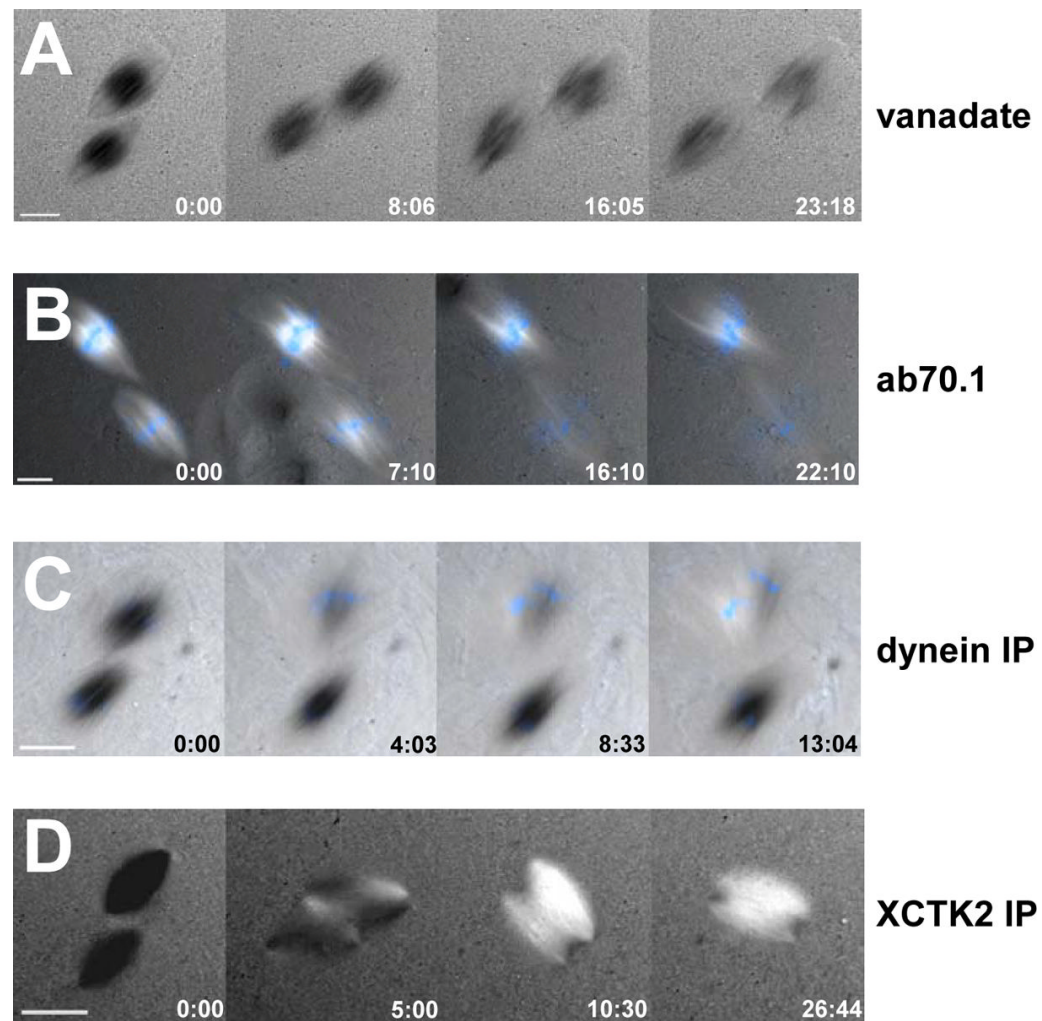


Figure 4. Dynein is required for bipolar spindle alignment and fusion

Polarization images of spindles pairs positioned with their proximal poles overlapped and their interpolar axes parallel to one another. Shown in **A** are images of bipolar fusion from a time-lapse series following addition of 25 μ M vanadate. In **B**, antibodies to dynein intermediate chain (final concentration $\sim 1.0 \text{ mgml}^{-1}$) were added 5-10 minutes prior to the start of imaging. Notice that spindle alignment and fusion fail under both experimental conditions. To confirm the requirement for dynein, the ability of micromanipulated spindles to fuse was assayed following assembly in immunodepleted extracts containing less than 2.5% of the endogenous protein (**C**; see Supplemental Data, Figure S2). In these assays, pairs of bipolar microtubule arrays, which lacked focused poles as expected, were positioned initially with their long axes parallel to one another and with overlapped birefringence. All perturbations of cytoplasmic dynein function completely blocked spindle fusion. In contrast, spindles assembled in XCTK2-depleted extracts still fused (**D**). Scale bars represent 25 μ m.

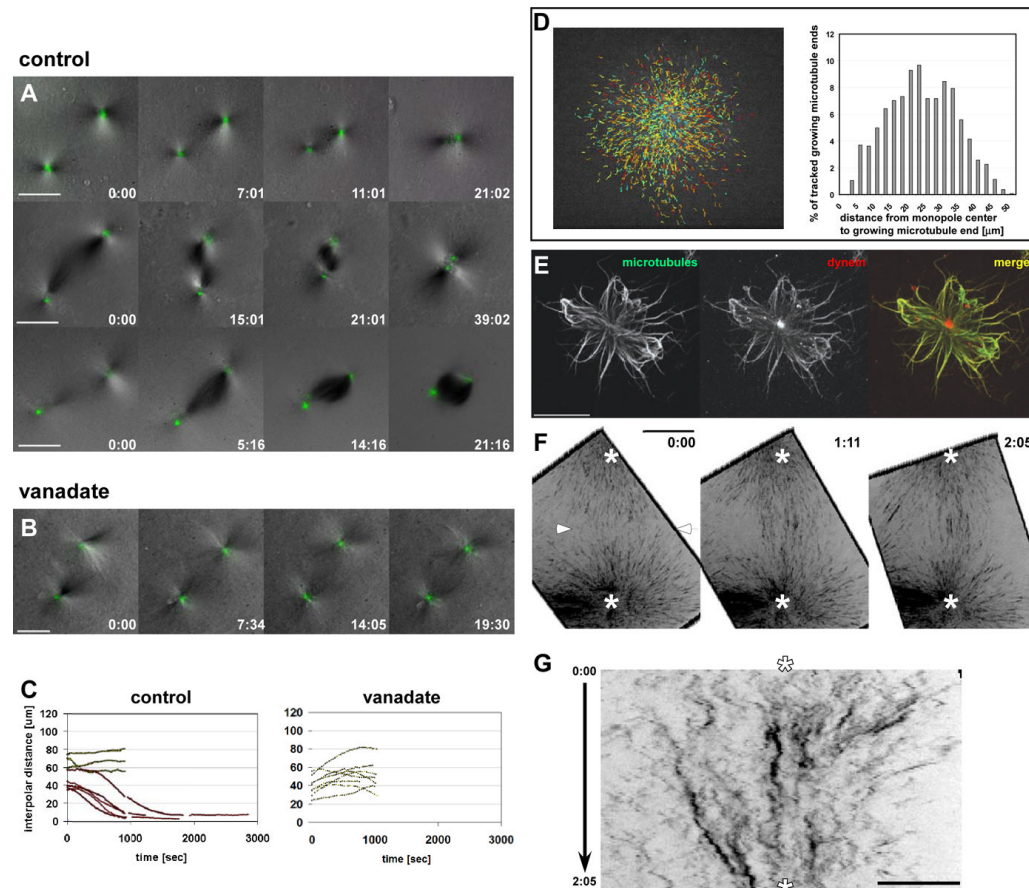


Figure 5. The fusion of Eg5-inhibited monopoles is mediated by dynein-dependent sliding of antiparallel microtubules

Following spindle assembly, *Xenopus* egg extracts were treated with the Eg5-specific inhibitors STLC (25μM) or monastrol (100μM). Poles were labeled with anti-NuMA antibodies conjugated to AlexaFluor 488 to facilitate automated pole tracking. Fusion was monitored using polarization optics and fluorescence microscopy. **A**, three examples of Eg5-inhibited monopole fusion demonstrating varying degrees of increased inter-polar birefringence observed during fusion (total $n > 20$ pairs). **B**, addition of 25μM vanadate (~5-10min prior to imaging) inhibited monaster fusion. For each experimental condition, the inter-polar distance between anti-NuMA labeled poles was plotted as a function of time (**C**). In these plots, the initial separations between monopole pairs are equal to the inter-polar distance values at time $t = 0$. **D**, growing microtubule plus ends were visualized by addition of 125 nM AlexaFluor 488-labeled EB1 and recorded using confocal microscopy. The image is a single frame selected from a ~2min time lapse recording overlaid with EB1 tracks ($n = 1396$ tracks with a minimum lifetime of 4 consecutive frames). The histogram shows the distribution of radial distances from the monopole center (see Materials and Methods) to the distal end of each EB1 track. In **E**, Eg5-inhibited monopoles were spun down on coverslips following fixation as described in [48]. The monopoles were then processed for immunofluorescence microscopy using antibodies against tubulin (green) and the 70.1/74 kDa intermediate chain of dynein (red). The extent and dynamics of microtubule plus ends during monopole fusion were assessed by labeling growing microtubule ends by adding 125nM GFP-EB1 to assembled monopoles (**F** and **G**; see Movie 2). The images in **F** (shown in inverted contrast) are from a time-lapse series of two monopoles, marked by asterisks, at the initial stages of interaction (a third monopole is out of the field towards the lower right). Microtubule density increases in a region half-way

between the poles. **G**, a kymograph of the linear region between the two arrowheads in **F** is used to show movements of EB1-labeled ends toward the interpolar axis (asterisks mark the approximate position of the poles). All scale bars represent a length of 25 μ m, except for the scale bar in panel **G**, which is equivalent to 10 μ m.

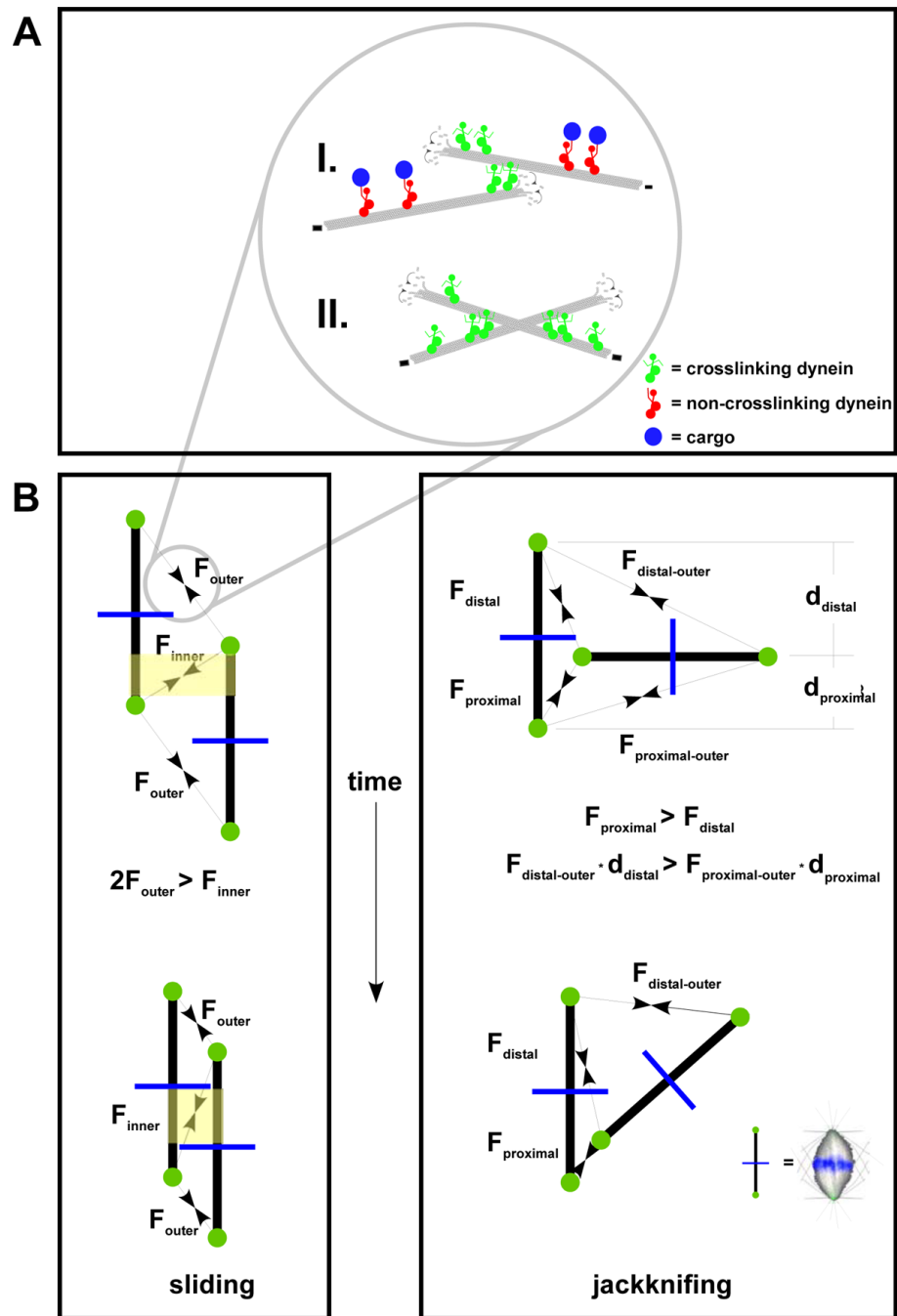


Figure 6. A model for bipolar spindle fusion

A, a cartoon schematic showing ways in which dynein-dependent sliding of antiparallel, peripheral microtubules might occur. These two models differ in that the first relies on plus end growth to license the dynein motor, permitting crosslinking only near growing plus ends. Whereas in the second, dynein crosslinking is independent of plus end growth and can occur anywhere along the length of the microtubule. **B**, dynein-dependent sliding of oppositely oriented, peripheral microtubules extending from each pole can account for both modes of bipolar spindle merging. For the sliding mode, we predict that the sum of forces generated between the outer pole of one spindle and inner pole of the other is greater than the attractive force between the two inner poles. Eg5-dependent sliding in regions of antiparallel overlap

between spindle microtubules (highlighted in yellow) might antagonize the dynein-mediated pulling forces, contributing to proximal pole separation. The jackknifing mode is more complex as it requires the generation of torque. In each of our “T-bone” experiments, the two nearest poles moved together first, likely due to F_{proximal} being greater than F_{distal} . However, this imbalance would not be expected to generate the torque required for the observed “jackknifing”. We propose that the initial geometry creates a mechanical advantage (i.e. longer lever arm) for $F_{\text{distal-outer}}$ thereby generating a torque that favors a rotation in the counter-clockwise direction as drawn.